Hybrid Gaussian–discrete-variable representation for one- and two-active-electron continuum calculations in molecules/article-title>

F. L. Yip, C. W. McCurdy, and T. N. Rescigno

Phys. Rev. A **90**, 063421 — Published 18 December 2014

DOI: 10.1103/PhysRevA.90.063421

Hybrid Gaussian-discrete variable representation for one- and two-active electron continuum calculations in molecules

F. L. Yip,[1] C. W. McCurdy,[2,3] and T. N. Rescigno[2]

[1]*Department of Science and Mathematics, California Maritime Academy, Vallejo, CA 94590, USA*
[2]*Lawrence Berkeley National Laboratory, Chemical Sciences, Berkeley, California 94720, USA*
[3]*Department of Chemistry, University of California, Davis, CA 95616 USA*

(Dated: December 3, 2014)

A combined basis of analytic Gaussian functions and grid-based FEM-DVR spherical harmonic expansion is specialized for description of continuum electron dynamics in the presence of electrons held fixed in core molecular orbitals. The applicability of this hybrid representation designed for general problems involving accurate determination of molecular continua wave functions is illustrated for photoionization of second-row diatomic molecules. Accurate descriptions of such electron continuum dynamics are a necessary step towards analyzing correlated double continua photoejections. Examination of this hybrid method in comparison to a more computationally expensive pure grid-based single center expansion reveals several key advantages that by design make it attractive for describing processes involving one or more electrons moved to the continuum.

I. INTRODUCTION

The ability to generate accurate descriptions of molecular continuum states for even the simplest molecules such as diatomics represents a non-trivial computational requirement for describing processes involving one or more electrons ejected from a molecule. Whether employing a basis of analytic functions or a numerical grid-based representation, describing electron dynamics in a molecule with oscillatory character that must be accurately represented over large reaches of physical space presents a significant challenge for theoretical methods. In fact, analytical basis functions such as Gaussian or Slater-type orbitals that are much better suited to exponentially-decaying bound states suffer significant pathologies arising from linear-dependence issues when trying to describe electronic continuum dynamics far from the nuclei. At the same time, a proper representation of these unbounded states is essential to theoretically describe photoionization processes that can elucidate the rich environment of molecules. In particular, the ability to probe electron correlation in molecular targets with many electrons via double ionization is both a lofty goal for theory and necessarily requires a faithful and robust means to describe even just single-electron ionization processes in the continuum.

Employing the Born-Oppenheimer approximation is a natural starting point for hoping to simplify any description of the electron dynamics, but it does not change the basic difficulties associated with having a non-spherical target. In particular, for any theoretical treatment that will accurately describe correlations between (at least) two electrons in a double photoionization event, grid-based approaches for atomic targets possess a spherical symmetry of the residual ionic center for which coupled spherical harmonics, known also as bi-polar harmonics $\mathcal{Y}^{L,M}_{l_1,l_2}(\hat{\mathbf{r}}_1,\hat{\mathbf{r}}_2)$, that couple radial equations provides a natural and efficient means to describe the continuum electron dynamics. For molecules, however, the off-center nature of more than one nucleus in the target requires accurately treating the cusps in the electronic wave function at the location of the nuclei [1]. For diatomic molecules, the natural extension of a spherical basis description leads to employing prolate-spheroidal or elliptical coordinate systems that by design allow for singularities at the foci. These coordinate systems also preserve the cylindrical symmetry of diatomics, and their use in calculating fully differential molecular frame double photoionization cross sections has been demonstrated [2–4].

In the general molecular case, however, lacking the ability to naturally resolve the electronic wave function cusps at the nuclei presents major challenges. Though one might hope that employing a single-center expansion in terms of a radial basis centered at the origin and spherical harmonics $Y^m_l(\hat{\mathbf{r}})$ for each electron might be feasible to describe electron dynamics for molecular targets, in practice it proves to be slowly convergent in the number of partial waves that must be used. A variety of radial functions, for example B-splines [5–9], have been utilized in describing the electronic continuum along these lines. Still, judicious choice of the location of the nuclei relative to the origin to maximize symmetry cannot avoid the general need for large l-components due to the non-spherical nature of molecules.

For single ionization of a valence electron in a molecule where only one electron need be represented in the continuum, this description is tractable with partial wave terms including up to $l_{\max} \sim 20$ to 50 being common. The manifestation of these large partial wave contributions to the molecular frame photoionization angular distribution (MFPAD), however, is not directly witnessed but rather impacts the lower partial waves that do directly contribute in the region immediately near the nuclei. Phrased another way, the resulting single ionization cross section requires accuracy in describing both the initial target state and the continuum final state, particularly in the vicinity of both the nuclei and the remaining target electrons to which both bound and continuum orbitals remain orthogonal [10, 11].

To employ such a single-center treatment for double ionization with each electron described by a large number of coupled partial waves is obviously impractical for any molecule heavier than H_2, where cross sections differential in both electron directions and energy sharing require up to $l_{\max} \sim 7$ to converge [12–15]. Under the conditions where the target becomes less spherical in nature (i.e., larger internuclear distance for the diatomic case, or more nuclei off-axis for polyatomics) or the cusps become more pronounced (larger Z at heavier atom centered), the tractability of this framework quickly worsens. Already such a relatively small number of partial waves to converge H_2 double ionization calculations provides a non-trivial computational challenge for which being able to treat a simple but chemically common diatomic like N_2 or O_2 would be prohibitively expensive in such a scheme.

In atomic double ionization, we have recently reported the ability to treat ejection of two valence electrons by representing them on a grid with full dimensionality in the field of the other non-ionized electrons. This has been demonstrated both where the non-ionized electrons form a spherically symmetric singlet closed-shell [16–18] and for atoms whose residual dication is left behind in open-shell configurations of various spin multiplicities [19, 20]. The results are remarkably accurate compared with experimental measurements, thus indicating that a first step to being able to treat double ionization in targets with more than only two electrons can proceed as long as: 1) electron correlation of those electrons to be moved into the continuum by the photoabsorption are treated precisely, and 2) the interaction of these outgoing electrons with those of the residual target be accounted for, at least, in an average way.

Prior to these findings, we have previously described a hybrid basis of Gaussian-type orbitals (GTOs) and discrete variable representation (DVR) functions as a basis for describing molecular processes where one or more electrons are moved into the continuum [21, 22]. The main advantage of such a hybrid basis is to merge the advantageous aspects of each basis where it is best suited for description of a molecular continuum wave function. This hybrid treatment relies on the use of: 1) Gaussian functions ubiquitous with molecular bound state wave function calculations to exclusively represent the region near the nuclei, and 2) an outer region of finite element DVR (FEM-DVR) and spherical harmonics aptly suited for describing continuum wave function oscillations far from the nuclei, i.e., where the residual target intermolecular distances are comparatively smaller than the radial distance from the molecular center of mass and the target left behind would appear to be more like a spherical point-charge of the residual cation. The key points in connecting these two bases to give the hybrid representation, as well as a demonstration of the advantages gained by letting appropriate Gaussian functions describe the electron wave function nuclear cusps to avoid the most limiting aspects of a pure single-center expansion FEM-DVR treatment, are discussed in more detail in Ref. [21].

In moving towards application of such a hybrid Gaussian-DVR framework for molecular double ionization, the ability to accurately determine single ionization continuum wave functions is not merely a test of the feasibility for the simpler one-electron problem, but a necessity within our double ionization treatment. These one-electron continuum functions, being orthogonal to the double ionization continuum solutions of the same residual Hamiltonian, serve as testing functions in matrix elements that extract the single ionization continuum that would otherwise contaminate the double ionization components [14, 23]. Thus, efficient and accurate representation of these non-trivial molecular continuum states for one-electron problems are a vital component of any progress towards molecular double ionization.

In this work we report application of the hybrid basis to molecular valence photoionization of fixed-nuclei targets with a single electron outside of a closed-shell core potential with many electrons. The relevance of the examples chosen, nitric oxide (NO) and the isoelectronic molecular oxygen cation (O_2^+), is to demonstrate accuracy with previous calculations [24–26] and advance towards employing such frozen-core strategies in a full double ionization framework where the single ionization continuum functions report here would serve as testing functions. In Section II, we discuss the construction of a molecular continuum wave function and provide a brief overview of the hybrid Gaussian-DVR method applied to NO and O_2^+. We also elaborate on the application of this continuum function in a photoionization context more complicated than previously considered. Results for partial cross sections and angular distributions, including MFPAD results are presented in Section III. Section IV concludes with a view towards these results in the context of the larger molecular double ionization problem.

II. THEORY

We begin with a brief overview of the key features of the hybrid Gaussian-DVR applied to the molecular environments of NO and O_2^+. More complete descriptions of the method applied to simpler diatomic molecules can be found in Refs. [21] and [22].

A. Hybrid description of molecular targets with occupied core electrons

As with double ionization from atomic targets in the presence of core electrons, we being by considering an anzatz wave function accounting for a proper description of the electron to be moved into the continuum with those (non-

active) electrons remaining behind in the target. For the molecular examples considered here, we treat photoionization of the outermost π orbital in the field of the core electrons. Considering a vertical transition from the ground Born-Oppenheimer electronic state of initial target to the photoionized cation, the overall process in NO is

$$\mathrm{NO}\ X\ ^2\Pi + h\nu \rightarrow \mathrm{NO}^+(2\pi^{-1})\ X\ ^1\Sigma + e^- \begin{cases} k\sigma \\ k\pi \\ k\delta \end{cases}, \tag{1}$$

and for O_2^+ is

$$\mathrm{O}_2^+\ X\ ^2\Pi_g + h\nu \rightarrow \mathrm{O}_2^{++}(1\pi_g^{-1})\ X\ ^1\Sigma_g + e^- \begin{cases} k\sigma_u \\ k\pi_u \\ k\delta_u \end{cases}, \tag{2}$$

where the dipole selection rules for linear molecules result in the polarization-dependent photoelectron continua shown (see Sec. II B below). For either molecular target shown above, the 14 core electrons are assumed to have the occupation $(1\sigma)^2(2\sigma)^2(3\sigma)^2(4\sigma)^2(5\sigma)^2(1\pi)^4$for NO, and $(1\sigma_g)^2(1\sigma_u)^2(2\sigma_g)^2(2\sigma_u)^2(3\sigma_g)^2(1\pi_u)^4$, for O_2^+. Construction of these core orbitals arises from solving the molecular Hartee-Fock equations using standard quantum chemistry basis sets. The atomic orbital bases that follow will range from minimal Slater-type orbitals (STO-3G) [27] to more elaborate correlation-consistent double- and triple-zeta bases for the nitrogen and oxygen atoms [28]. The interaction of these core electrons with the ejected valence photoelectron is taken at the static-exchange level with those occupied core orbitals shown above. In this simplified multi-electron picture, the role of those electrons not ionized by the photon is to screen the bare nuclei and provide an appropriate closed-shell non-local exchange interaction. The approximation that the core orbitals do not relax during the photoionization (frozen-core approximation) is also assumed in the descriptions that follow.

The effective one-electron Hamiltonian for the photoionizing electron for either molecular target is (in atomic units)

$$H = T + V_{\mathrm{nuc}} + \sum_{\mathrm{occ}} (2J - K), \tag{3}$$

where

$$\begin{aligned} T &= -\frac{1}{2}\nabla^2, \\ V_{\mathrm{nuc}} &= -\frac{Z_A}{|\mathbf{r} - \mathbf{R_A}|} - \frac{Z_B}{|\mathbf{r} - \mathbf{R_B}|}, \end{aligned} \tag{4}$$

are the kinetic energy and nuclear attraction operators, respectively. The bare nuclei, labeled A and B above, possess charges Z_A and Z_B and are located along the molecular axis (defined to be the z-axis in the body-fixed frame) at mass-weighted distances from the origin along the molecular axis. The interaction of the 14 core electrons with the valence electron is included via the closed-shell static exchange potential where J represents the Coulomb (direct) operator and K is the non-local exchange operator.

The one-body Hamiltonian above requires construction of these operators in the hybrid Gaussian basis. For each operator, the matrix elements must be calculated between bra and ket of three distinct possible combinations: 1) two Gaussian $\langle G_i|\hat{O}|G_j\rangle$, 2) two DVR functions $\langle \chi_i|\hat{O}|\chi_j\rangle$, and 3) a mixed case with one Gaussian and one DVR function $\langle G_i|\hat{O}|\chi_j\rangle$. The details of constructing the kinetic energy and nuclear attraction operators in Eq. 3 in the hybrid Gaussian scheme are given in Ref. [21]. Below we focus on the construction of the occupied-core potential.

The construction of the direct and exchange contributions from an *a priori* defined occupied closed-shell core can be constructed from the one-particle density matrix

$$\rho_{k,l} = \sum_{\mathrm{occ}} c_k^{\mathrm{occ}} c_l^{\mathrm{occ}}, \tag{5}$$

with an underlying basis of occupied molecular orbitals determined from, for example, a closed-shell Hartree Fock calculation with the k-th molecular orbital expansion coefficients c_k exported from an external molecular structure code. The underlying basis for construction of these molecular orbitals consists of Gaussian-type orbitals and, for simplicity, can provide a beginning point for determination of the GTOs used to construct the valence orbital in the hybrid scheme.

By employing molecular orbitals defined from an underlying Gaussian basis, the possible classes of mixed basis two-electron integrals involving either GTOs or DVR functions must be considered. A full discussion of the complete list of classes in this hybrid basis framework and detailed derivations of the computational strategy for evaluating these two-electron integrals can be found in Ref. [22]. Below we explore the convergence issues for the most complicated class of mixed-basis integrals and the consequences of having heavier nuclei with many more core electrons than previously considered.

Here we focus on two of the most commonly occurring classes which highlight the interface of the analytic Gaussian and grid-based description of the electronic coordinates. These will involve one-electron matrix elements of the occupied core, represented in Gaussian MOs, taken between two DVR functions. The Gaussian basis functions are labeled as $G_i(\mathbf{r})$ and the DVR basis functions (in full dimensionality) are denoted

$$\chi^a_j(\mathbf{r}) = r^{-1}\phi_j(r)Y_{l^a,m^a}(\hat{\mathbf{r}}) \tag{6}$$

in what follows. The Coulomb operator between two DVR functions given by,

$$\langle\chi^a_i|J|\chi^b_j\rangle = \sum_{k,l}\rho_{k,l}\langle\chi^a_i G_k|\chi^b_j G_l\rangle, \tag{7}$$

involves Class 3 two-electron integrals $\langle\chi^a_i G_k|\chi^b_j G_l\rangle$ as enumerated in Ref. [22], representing a mixed description where one of the electrons is represented by only DVR functions and the other only by Gaussians. The related exchange operator between two DVR functions is

$$\langle\chi^a_i|K|\chi^b_j\rangle\sum_{k,l}\rho_{k,l}\langle\chi^a_i G_k|G_j\chi^b_l\rangle, \tag{8}$$

which involves the two-electron integrals $\langle\chi^a_i G_k|G_j\chi^b_l\rangle$ labeled as Class 4 integrals in Ref. [22], where each electron is described by both a Gaussian and DVR function. These two classes represent a significant number of hybrid basis two-electron integrals that must be evaluated to construct occupied core potential of the Hamiltonian in Eq. 3

The strategy for evaluating the Class 3 integrals, those involving the same type of hybrid basis function in the coordinates of the same electron, involves representing the two-body repulsion $1/r_{12}$ between two GTOs of the same electron as a local potential of the other electron,

$$I_{k,l}(\mathbf{r}_1) \equiv \int G_k(\mathbf{r}_2)\frac{1}{r_{12}}G_l(\mathbf{r}_2)\; d\mathbf{r}_2\,. \tag{9}$$

Thus the two-electron integral in Eq. 7 becomes

$$\begin{aligned}\langle\chi^a_i G_k|\chi^b_j G_l\rangle &= \int\left(\int G_k(\mathbf{r}_2)\frac{1}{r_{12}}G_l(\mathbf{r}_2)\; d\mathbf{r}_2\right)\\ &\qquad\times\chi^{a*}_i(\mathbf{r}_1)\chi^b_j(\mathbf{r}_1)\; d\mathbf{r}_1\\ &= \int I_{k,l}(\mathbf{r}_1)\chi^{a*}_i(\mathbf{r}_1)\chi^b_j(\mathbf{r}_1)\; d\mathbf{r}_1\,,\end{aligned} \tag{10}$$

which, due to the properties of the DVR when integrated over the radial coordinates of $\mathbf{r}_1$, reduces the matrix element to an angular integration over a shell,

$$\begin{aligned}\langle\chi^a_i G_k|\chi^b_j G_l\rangle &= \int I_{k,l}(\mathbf{r}_1)\frac{\phi_i(r_1)}{r_1}Y^*_{\ell^a,m^a}(\hat{\mathbf{r}}_1)\\ &\qquad\times\frac{\phi_j(r_1)}{r_1}Y_{\ell^b,m^b}(\hat{\mathbf{r}}_1)\; d\mathbf{r}_1\\ &= \delta_{i,j}\int I_{k,l}(r_j;\hat{\mathbf{r}}_1)Y^*_{\ell^a,m^a}(\hat{\mathbf{r}}_1)Y_{\ell^b,m^b}(\hat{\mathbf{r}}_1)\; d\hat{\mathbf{r}}_1\,,\end{aligned} \tag{11}$$

that can be performed with a suitable angular quadrature rule [29].

More difficult is the class of exchange two-electron integrals of Eq. 7 that have both a GTO and a DVR function describing both electrons. The difficulty then becomes to accurately represent the two-electron density accurately enough to employ a multipole expansion,

$$\frac{1}{r_{12}} \equiv \frac{1}{|\mathbf{r}_1-\mathbf{r}_2|} = \sum_{\lambda,\mu}\frac{4\pi}{2\lambda+1}Y_{\lambda,\mu}(\hat{\mathbf{r}}_1)\frac{r^\lambda_<}{r^{\lambda+1}_>}Y^*_{\lambda,\mu}(\hat{\mathbf{r}}_2)\,, \tag{12}$$

and perform a single-center expansion of the radial Gaussian density as

$$rG_i(\mathbf{r})Y_{l',m'}(\hat{\mathbf{r}}) = \sum_{l,m} R_{l,m}^{i,l',m'}(r)Y_{l,m}(\hat{\mathbf{r}})\,, \tag{13}$$

with expansion coefficients given by

$$R_{l,m}^{i,l',m'}(r) = r\int G_i(\hat{\mathbf{r}};r)Y_{l',m'}(\hat{\mathbf{r}})Y_{l,m}(\hat{\mathbf{r}})\;d\hat{\mathbf{r}}\,. \tag{14}$$

Using this expansion basis and the orthonormality of the spherical harmonics gives the resulting expansion,

$$\begin{aligned}\langle\chi_i^a G_k|G_j\chi_l^b\rangle =& \sum_{\lambda,\mu}\frac{4\pi}{2\lambda+1}\sum_{l_1,m_1}\sum_{l_2,m_2}\delta_{l_1,\lambda}\delta_{m_1,\mu}\delta_{l_2,\lambda}\delta_{m_2,\mu}\left[\int R_{l_1,m_1}^{j,\ell^a,m^a}(r_1)\phi_i(r_1)\frac{r_<^\lambda}{r_>^{\lambda+1}}R_{l_2,m_2}^{k,\ell^b,m^b}(r_2)\phi_l(r_2)\;dr_1\;dr_2\right]\\ =& \sum_{\lambda,\mu}\frac{4\pi}{2\lambda+1}\int R_{\lambda,\mu}^{j,\ell^a,m^a}(r_1)\phi_k(r_1)\frac{r_<^\lambda}{r_>^{\lambda+1}}R_{\lambda,\mu}^{k,\ell^b,m^b}(r_2)\phi_l(r_2)\;dr_1\;dr_2\,.\end{aligned} \tag{15}$$

As detailed in Ref. [23], the radial integrals cannot be accurately calculated using the underlying DVR quadrature rules. Instead, the radial density of each expansion term is recast into

$$\begin{aligned}&\int R_{l_1,m_1}^{j,\ell^a,m^a}(r_1)\phi_i(r_1)\frac{r_<^\lambda}{r_>^{\lambda+1}}R_{l_2,m_2}^{k,\ell^,m^b}(r_2)\phi_l(r_2)\;dr_1\;dr_2\\ &\qquad\qquad = \left\langle\rho_1\left|\frac{r_<^\lambda}{r_>^{\lambda+1}}\right|\rho_2\right\rangle\end{aligned} \tag{16}$$

in order to find a solution of Poisson's equation that can be re-expanded in the underlying radial DVR basis. The derivation parallels a similar treatment of the multipole expansion of the two-body repulsion term with only DVR grid functions [23]. The final result of this hybrid basis two-electron density repulsion is found to be

$$\begin{aligned}\left\langle\rho_1\left|\frac{r_<^\lambda}{r_>^{\lambda+1}}\right|\rho_2\right\rangle =& (2\lambda+1)\left[\frac{R_{\lambda,\mu}^{j,\ell^a,m^a}(r_i)}{r_i}\frac{R_{\lambda,\mu}^{k,\ell^b,m^b}(r_l)}{r_l}\right]\left[T_{i,l}^\lambda\right]^{-1} + \left(\frac{r_0^{2\lambda+1}-r_l^{2\lambda+1}}{r_0^{2\lambda+1}-r_{\max}^{2\lambda+1}}\right)\frac{R_{\lambda,\mu}^{j,\ell^a,m^a}(r_i)R_{\lambda,\mu}^{k,\ell^b,m^b}(r_l)\sqrt{w_iw_l}r_i^\lambda}{r_l^{\lambda+1}}\\ &+\left(\frac{r_l^{2\lambda+1}-r_{\max}^{2\lambda+1}}{r_0^{2\lambda+1}-r_{\max}^{2\lambda+1}}\right)\frac{R_{\lambda,\mu}^{j,\ell^a,m^a}(r_i)R_{\lambda,\mu}^{k,\ell^b,m^b}(r_l)\sqrt{w_iw_l}r_0^{2\lambda+1}}{(r_ir_l)^{\lambda+1}}\,,\end{aligned} \tag{17}$$

where $\left[T_{i,l}^\lambda\right]^{-1}$ is the inverse of the radial kinetic energy matrix including the λ-dependent centrifugal barrier, w_i and w_l are the associated Lobatto quadrature weights for FEM-DVR points r_i and r_l, respectively [30]. It follows that the last two terms in Eq. 17 are surface terms due to the boundary conditions for which the first and last radial points are denoted r_0 and $r_{\max}$, respectively.

Although the similarities between this result and the simpler two-electron radial repulsion involving only pure DVR functions are apparent, one significant difference is that due to the single-center expansion of the Gaussian functions according to Eq. 14, the multipole sum of Eq. 15 does not truncate. In fact, one can anticipate that larger Gaussian exponents of "tighter" inner-shell orbitals will be most affected by higher λ terms. This point will be re-addressed when comparing the hybrid Gaussian results with a pure single-center DVR expansion.

It should also be mentioned that though the DVR region extends to the end of the radial grid, the extent of the exchange component only possesses the range of the core orbitals and thus, the computationally demanding Class 4 matrix elements between mixed Gaussian and DVR functions can be limited to those finite elements where the occupied orbitals have non-negligible extent and safely assumed to be zero at larger radial distances. This is contrasted with the direct Coulomb terms of Eq. 7 whose long range nature is critical to screen the attractive nuclear centers at large distances.

B. Calculation of molecular photoionization amplitudes using the hybrid basis

With the framework for constructing the molecular Hamiltonian discussed, we turn our attention to using the hybrid Gaussian-DVR basis to construct continuum wave functions appropriate for treating the valence photoionization.

These continuum states are defined by a total energy E and an outgoing momentum $\mathbf{k}$ of the ejected photoelectron. By referencing the energy scale to the frozen-core energy (i.e., setting the zero point at the ionization threshold of the valence π electron), these continuum states will satisfy

$$\left[H - \frac{k^2}{2}\right] \Phi^{(+)}(\mathbf{k}, \mathbf{r}) = 0\,. \tag{18}$$

The outgoing wave boundary conditions are imposed by solving this equation for a Hamiltonian constructed with exterior complex scaling (ECS) and solving the following associated driven equations along a complex radial contour [23]. The photoionization cross section for ejecting an electron with momentum $\mathbf{k}$ in the molecular frame defined by the internuclear axis along direction $\hat{\mathbf{A}}$ is given by

$$\sigma(\mathbf{k}, \epsilon, \hat{\mathbf{A}}) = 4\pi^2 \frac{\omega k}{c} \left| \left\langle \Phi^{(-)}(\mathbf{k}, \mathbf{r}) \middle| \epsilon \cdot \mathbf{r} \middle| \Phi_0(\mathbf{r}) \right\rangle \right|^2 , \tag{19}$$

where ω is the photon energy, ϵ is the photon polarization direction relative to the molecular axis (coincident with the z-axis), $\Phi_0(\mathbf{r})$ is the molecular initial state, and $\Phi^{(-)}(\mathbf{k}, \mathbf{r})$ is the (incoming) molecular continuum wave function, satisfying the relation

$$\Phi^{(-)}(\mathbf{k}, \mathbf{r}) = \left[\Phi^{(+)}(-\mathbf{k}, \mathbf{r})\right]^* , \tag{20}$$

of the solutions of Eq. 18. The dipole operator, shown in the length gauge above, determines the possible molecular continuum state symmetries for the photoelectron as shown in Eqs. 1 and 2 for NO and O_2^+, respectively.

Following our previous prescription of determining these continuum states and utilizing them in equivalent surface integrals at relatively large radial distances just inside of the ECS complex rotation point [23], we partition the outgoing wave as

$$\Phi^{(+)}(\mathbf{k}, \mathbf{r}) = \xi(\mathbf{k}, \mathbf{r}) + g(r) \Psi_c^{(+)}(\mathbf{k}, \mathbf{r})\,, \tag{21}$$

where $\Psi_c^{(+)}(\mathbf{k}, \mathbf{r})$ is an outgoing Coulomb wave given by

$$\begin{aligned} \Psi_{\rm c}^{(+)}(\mathbf{k}, \mathbf{r}) =& (2\pi)^{-3/2} e^{\pi Z/2k} e^{i\mathbf{k}\cdot\mathbf{r}} \Gamma(1 - iZ/k) \\ & {}_1F_1(+iZ/k; 1; i(kr - \mathbf{k}\cdot\mathbf{r}))\,, \end{aligned} \tag{22}$$

with $Z = 1$ for NO and $Z = 2$ for O_2^+ seen as a point-like source in the asymptotic region, but attenuated by a smooth but otherwise arbitrary function $g(r)$ that approaches unity at large r and cuts off the Coulomb function for smaller r. Since the outer DVR region of the hybrid scheme has angular coordinates represented in spherical harmonics, it is convenient to use a partial wave Coulomb expansion,

$$\Psi_c^{(+)}(\mathbf{k}, \mathbf{r}) = \left(\frac{2}{\pi}\right)^{1/2} \sum_{l,m} i^l e^{i\eta_l(k)} Y_{l,m}^*(\hat{\mathbf{k}}) \frac{\phi_{l,k}^{(\rm c)}(r)}{kr}\,, \tag{23}$$

with radial Coulomb waves $\phi_{l,k}^{(\rm c)}(r)$ that behave asymptotically as $\sin\left(kr + (Z/k)\ln 2kr - \pi l/2 + \eta_l(k)\right)$, possessing Coulomb phase shift $\eta_l(k) = \arg\Gamma(l + 1 + iZ/k)$.

To fully determine the three-dimensional outgoing wave in Eq. 21, we represent the undetermined portion $\xi(\mathbf{k}, \mathbf{r})$ for the photoelectron $\mathbf{k}$ as a spatial function expanded in the hybrid Gaussian-DVR basis for some incoming partial wave channel l_0

$$\begin{aligned} \frac{\xi(\mathbf{r})^{l_0,m}}{r} &= \sum_\Gamma c_\Gamma^{l_0,m} G_\Gamma(\mathbf{r}) + \sum_{i,l} c_{il}^{l_0,m} \frac{\chi_i(r)}{r} Y_{l,m}(\hat{\mathbf{r}}) \\ &\equiv \sum_\Gamma c_\Gamma^{l_0,m} G_\Gamma(\mathbf{r}) + \sum_l \frac{P_l^{l_0,m}(r)}{r} Y_{l,m}(\hat{\mathbf{r}})\,, \end{aligned} \tag{24}$$

where the index Γ labels the Gaussian type functions coupled to l_0, $P_l^{l_0,m}(r)$ defines a radial function that will augment the long-range portion of Eq. 21 in channel l_0, and we have used the fact that m is a good quantum number in cylindrical symmetry. This partial wave decomposition leads to a set of driven equations for each incoming l_0, m Coulomb wave channel,

$$\left(\frac{k^2}{2} - H\right) \frac{\xi^{l_0,m}(\mathbf{r})}{r} = \left(H - \frac{k^2}{2}\right) g(r) \frac{\phi_{l_0,k}^{(c)}(r)}{r} Y_{l_0,m}(\hat{\mathbf{r}})\,. \tag{25}$$

Utilizing a hybrid basis expansion as in Eq. 24 to solve these equations reveals the contributions associated with the outer DVR region $P_l^{l_0,m}(r)$ that will describe the photoionization event, since by choosing the cutoff function $g(r)$ to decay in the region of the Gaussian functions eliminates the contributions from this part of the basis to the continuum representation at large r. The advantage gained is avoidance of rotating the analytical Gaussian functions into the complex ECS contour, relying solely on the (practically complete) grid-based DVR functions to capture the wave function dynamics beyond the Gaussian orbital extent.

Figure 1 presents a few continuum wave solution constructed in the hybrid Gaussian-DVR basis for valence photoionization from NO to produce a 10 eV photoelectron in both parallel and perpendicular photon polarizations. Examining these wave functions plotted in the xz-plane of the molecule highlights the general features of this hybrid representation with Gaussians exclusively used to represent the electronic coordinates immediately near the nuclei and DVR grid functions with relatively few partial wave terms describing the oscillatory behavior beyond the Gaussian region. These examples illustrate the advantages of a hybrid method to construct molecular continuum wave functions through seamlessly merging the distinct underlying representations of the electron dynamics across those areas of physical space where they are appropriately utilized.

The continuum solutions like those presented in Figure 1 can be used to generate the body-fixed photoionization amplitude of Eq. 19 by performing a volume integral just within the ECS contour. Alternatively, the photoionization amplitude can be can be computed as a surface integral of a scattered wave solution that satisfies the driven equation

$$\Big[E - H\Big]\Psi_{\rm sc} = (\epsilon \cdot \mathbf{r})\Psi_0\,, \tag{26}$$

where again the total energy $E = E_0 + \omega$ is referenced to the orbital ionization potential of the valence electron, E_0. The scattered wave $\Psi_{\rm sc}$ is determined from the Green's function of $(E - H)$. Following this approach, for which a more detailed description can be found in ref. [23], we arrive at an equivalent form of the photoionization amplitude in terms of the partial-wave decomposed scattered states $P_{l'}^{l,m}(r)$,

$$\begin{aligned}
\big\langle \Phi^{(-)}(\mathbf{k},\mathbf{r})\big|E-H\big|\Psi_{\rm sc}(\mathbf{r})\big\rangle &= \frac{1}{2}\int_S \left[{\Phi^{(-)}}^*(\mathbf{k},\mathbf{r})\nabla\Psi_{\rm sc} - \Psi_{\rm sc}\nabla{\Phi^{(-)}}^*(\mathbf{k},\mathbf{r})\right]\cdot d\mathbf{S} \\
&= \frac{1}{2}\sqrt{\frac{2}{\pi}}\sum_{l,m} i^l e^{i\eta_l(k)} Y_{l,m}(\hat{\mathbf{k}}) \\
&\times \sum_{l'}\left\{\left[\frac{\phi_{l,k}^{(\rm c)}(r)}{kr}\delta_{l,l'} + \frac{P_{l'}^{l,m}(r)}{r}\right]\frac{d}{dr}\frac{\psi_{\rm sc}^{l',m}(r)}{r} - \frac{\psi_{\rm sc}^{l',m}(r)}{r}\frac{d}{dr}\left[\frac{\phi_{l,k}^{(\rm c)}(r)}{kr}\delta_{l,l'} + \frac{P_{l'}^{l,m}(r)}{r}\right]\right\} r^2\Bigg|_{r=S}\,.
\end{aligned} \tag{27}$$

This equivalent surface integral formulation has been used for single and double ionization from both atoms and molecules and reduces the dimensionality of calculating the ionization amplitude. With this expression for the ionization amplitude, we can consider molecular-frame photoionization from an oriented target and integrate over directions to produce partial cross sections for each particular m value of the final state dipole-connected to the π valence electron.

III. HYBRID BASIS CALCULATIONS OF MOLECULAR PHOTOIONIZATION IN NO AND O_2^+

The question of choosing a proper core molecular orbital representation for an ionization event is a common one because of the sensitivity of the continuum wave function to details of the residual target, particularly if relaxation effects are not considered through holding the core orbitals fixed, as we do here. The consequences of approximating the non-relaxed target orbitals by either those of the neutral molecule or those of the ionized core can impact the vertical ionization potential and the location or resolution of electronic structure in the calculated cross sections. Being able to represent the photoionization process in single ionization of a molecule, however, is necessary if these methods are to have any success at approximating the molecular environment where two electrons enter the continuum. Photoionization of the valence electron from nitric oxide provides a good test case as to the viability of this framework and provides an opportunity for comparison with other theoretical treatments.

Figure 2 displays the partial photoionization cross sections from NO calculated using the hybrid Gaussian-DVR treatment at the equilibrium internuclear distance, $R = 2.174$ a$_0$. Several different molecular orbital basis representations of the inner electrons have been used to construct the static-exchange potential, as shown. These results show good agreement in the magnitude and behavior of the partial cross sections for a variety of core-orbital representations. Using relatively simple basis sets derived from an SCF on the closed-shell NO^+ (curves without symbols) gives good agreement with larger basis set treatments derived from the natural orbitals of NO (curves with symbols), particularly

for the parallel-polarization $k\pi$ and perpendicular-polarization $k\delta$ partial continua. The effects of using ion orbitals versus neutral orbitals for the core potential are generally more important nearer to threshold and particularly more pronounced in the perpendicular polarization $k\sigma$ partial cross section, where a shape resonance feature is apparent at low photoelectron energy. The use of ion orbitals seems to produce the resonance peak at a few eV higher than is seen for neutral orbitals of NO. Though not shown here, this result is also observed using the same basis set designations for both the ion orbitals as for the neutral orbitals, and thus seems more related to the different ionization potentials of the 2π electron that arise from utilizing ion orbitals (9.6 eV for a minimum basis set, for example) as opposed to neutral orbitals (10.2 eV for the same minimum basis set).

Also shown in Fig. 2 are static-exchange results calculated with the Schwinger variational method [24] and the linear algebraic approach [25]. There is good agreement in those calculated cross section with results presented here. Focusing on the comparison between the general features of the different theoretical methods highlights two noteworthy results: first, that the resonance feature in the $k\sigma$ continuum is fairly well represented in the hybrid basis continuum description for all of the core-orbital basis representations and, second, that even a minimal basis set treatment using ion orbitals provides particularly good agreement with more extended basis sets and with the other theoretical results. These results indicate not only that the hybrid basis is viable for describing molecular continuum states, but are also encouraging in that even simple molecular orbital constructions of the frozen-core potential can capture the electron dynamics in the field of the molecular environment to a reasonable degree. Good agreement with these benchmarks are almost a necessity if this framework should have promise towards application for describing molecular double ionization.

To explore the success with which the underlying Gaussian basis functions of the inner region provide a significant advantage for molecular problems, we can compare these results with those calculated in a pure DVR single-center expansion. To do so, the closed-shell core potential of Eq. 3 is expanded in a molecular orbital basis with only radial DVR functions centered on the origin used to compute the direct and exchange operators as in Eqs. 7 and 8, respectively. The only modification of the working equations presented here is to set the starting point of the radial grid r_0 at the origin, which changes the surface terms in the radial exchange formulation of Eq. 17.

Figure 3 shows a comparison of the partial photoionization cross section of NO for the hybrid Gaussian-DVR and pure single-center DVR using both a minimum-basis core potential of the ion (upper panel) and more extended basis set construction of the neutral MOs (lower panel). Contrasting the computational details of each method illustrates the advantage of employing the hybrid scheme, where the results shown were calculated for each core potential with ~ 30 total interior region Gaussians of s-, p- and d-type and in the outer DVR region angular momentum terms with $l_{\max} = 5$ for each continua. However, for the pure DVR single-center expansion, the results presented are calculated with higher partial wave components of up to $l_{\max} = 9$ for the $k\pi$ and $k\delta$ symmetries, and up to $l_{\max} = 13$ for the $k\sigma$ results. Both calculations feature similar radial DVR grids of 17th-order FEM-DVR in five or six finite elements up to a common ECS scaling point at $R_0 = 35$ bohr. As expected, constructing the molecular wave function in the vicinity of nuclei about a single center now requires substantially more partial wave terms due to the nuclear attraction, as well as to represent the innermost core-orbital potentials. For both bases considered, agreement between the hybrid Gaussian-DVR and pure single-centered DVR is better for the $k\pi$ and $k\delta$ channels; the $k\sigma$ partial cross section features greater discrepancy with the hybrid method and less agreement with the other theoretical result shown, particularly in the magnitude of the resonance being larger and further in energy from the SV calculation results. This final-state symmetry is particularly sensitive to the cusps lying along the molecular axis. Utilizing the ion-orbital minimum basis shows greater agreement for all partial cross sections with the hybrid framework, perhaps due to the lack of larger orbital exponent values in the underlying MO core-orbital expansion basis.

Further examination of these distinct continuum wave function descriptions can be examined by comparing the plotted hybrid wave function of Fig. 1 with the pure DVR result of Fig. 4. The visualizations of these continuum states are of those that were used to generate the partial cross sections of the lower panel of Fig. 3 describing ionization from NO in the presence of the occupied core constructed in a ccvdz basis with the parameters shown above. For parallel polarization leading to the $k\pi$ continuum, the wave functions appear to differ most near the nuclei, while the oscillating character at larger radial distances up to the edge of the grid appear to be in substantial agreement. The partial cross sections in this channel also correlate fairly well with each other in shape, with some slight difference in the peak value of the cross section in magnitude and photoelectron energy location. This trend in the partial cross sections is also seen in the $k\delta$ final state channel as well.

A more substantial difference in the cross section is seen in the resonance feature of $k\sigma$ symmetry. Examining the lower panels of Fig. 1 and Fig. 4 containing the perpendicular polarization continuum state reveals similar wave function features overall, though larger values of the overall magnitude of the pure DVR representation near the nuclear cusps. The d-wave fringes directed towards the corners of the grid in the outer radial region show similar behavior in both cases, but examination of the behavior along the z-axis does reveal some differences. The contours projected below each two-dimensional wave function plot reveal small distinctions along the z-axis near the nuclei.

To better examine the characteristics of these continuum wave functions and the impact of the different symmetry-

dependent ionization channels populated by different photon polarizations, Figure 5 shows color-gradient scales of the results in Figs. 1 and 4 plotted in the xz-plane. For parallel polarization (leftmost figures), both the hybrid Gaussian-DVR and pure-DVR results show comparable fringe patterns in the outer region while differing most significantly near the nuclei. However, these inner region differences seem to bear less impact on the resulting cross section results in this symmetry because the node character along the z-axis excludes the nuclei, where differences in the ability to expand the wave function cusps are distinguished. In the perpendicular direction, despite the differences in the magnitude of the outer fringes compared to the inner region maxima, the d-wave character that contributes to the more similar $k\delta$ cross section results is in better agreement between the two treatments. For the $k\sigma$ continua, though the differences between the hybrid and pure single-center are subtle, they do seem to be more impactful on the resulting cross sections. This tends to indicate that the perpendicular polarization results and, in general, those directed along the nuclei will be most strongly influenced by the molecular environment and the manner in which it is described.

What is also apparent in comparing these visual plots of the electronic continua behavior is the impact of the partial wave terms both near the nuclei and in the asymptotic region. The contour plots of Fig. 5 highlight in particular that though the inner region might be particularly sensitive to the effects of the nuclei and the inclusion of high-order partial waves that is common to converge single-center expansion calculations, the outer region reveals little direct signature of their more complicated structure [10, 11]. It is particularly this observation that makes the hybrid Gaussian-DVR representation attractive, since many fewer partial waves are actually significantly important to resolve the nodal and oscillatory structure of the wave function at larger radial distances where the outgoing character is probed for the continuum dynamics. In fact, employing a modified pure single-center expansion with DVR functions featuring high-order spherical harmonics over the first few finite elements containing and just beyond the nuclei but truncated in the outer region gives results indistinguishable from those maintaining all higher partial waves over the entire radial space. Examination of the absolute magnitude of the photoionization amplitudes evaluated at large r reveal increasingly insignificant direct contribution to the asymptotic behavior (as seen in these wave function plots presented), but omitting the higher-order partial wave terms altogether destroys their impact on those lower-order partial waves that do contribute, damaging the photoionization angular distributions. Thus, the large l contributions are responsible for ensuring that the fewer significant partial wave terms that do contribute to the scattering are accurate in the vicinity of the nuclei and, consequently, in the outer region. This further highlights the natural advantage that make the hybrid Gaussian-DVR representation attractive for use in molecular continua problems.

The formulation of the hybrid Gaussian-DVR scheme to produce photoionization cross sections in full dimensionality allows for the examination of angular-dependent features in the body frame. With foresight towards being able to calculate such molecular frame information in order to compare with kinematically complete experimental techniques that can reconstruct the body-fixed frame for double ionization, the resolution of MFPAD results should also be examined. Figure 6 shows the differential cross section for photoionization of NO to produce a 10 eV photoelectron in the body frame with the molecular orientation along the horizontal z-axis. The photoelectron distribution is shown in the xz-plane ($\phi = 0$). The absolute cross section calculated in both the hybrid Gaussian-DVR scheme (solid curves) and with the pure DVR representation (dashed curves) are both shown. To compare the resulting angular distributions, the rightmost panels show polar plots normalized to the maximum value of each cross section from the corresponding panel at left.

The MFPAD for parallel polarization (upper panels of Fig. 6) reveal good agreement between the two calculations where again the hybrid method requires a much lower number total partial wave terms in the DVR region to yield the similar results of the pure DVR single-center expansion. Slight differences in the height of the peaks is seen between the calculations, but the normalized results show excellent agreement, with both revealing larger lobes directed closer towards the oxygen atom in this oriented target. More significant variations between these two results are revealed using x-polarized photons (lower panels). The prominent peaks of both calculations agree fairly well, but the pure-DVR result significantly underestimates cross section along the bond axis compared to the hybrid results. This is consistent with the larger discrepancy in the $k\sigma$ partial cross section at the tail of the resonance feature. Increasing the number of partial waves in the pure single-center expansion reveals a slowly converging change in this minor peak towards the hybrid Gaussian-DVR result, which do not change significantly with additional partial waves in the DVR region. Much better agreement in the larger peaks is seen in the normalized angular distribution, which are dominated by the d-wave contributions where the partial cross sections trend better and no resonance feature is present. Using x-polarized light now enhances the nitrogen-side prominent lobes in the MFPAD for both results. Overall, parallel polarization results between these two calculations show less influence of the region near the nuclei than perpendicular polarization.

The results for NO provide a benchmark to discuss these two methods and compare with other theoretical results. Finally, we wish to consider the analogous photoionization results for the isoelectronic O_2^+ molecule calculated at equilibrium internuclear distance $R = 2.11$ a$_0$. The ability to construct accurate continuum wave functions for this molecular ion is crucial in order to apply it as a single-ionization testing function for analysis of a double-ionization event of neutral O_2. Two distinctions between the NO and O_2^+ that might impact a comparison of the two results

should be mentioned. First, the cationic charge of the target for O_2^+ and, thus the twice-as-large residual charge of the ionic core potential should diminish the relative importance of the direct and exchange potentials at the expense of the nuclear attraction term. The continuum states determined from the driven equations like Eq. 25 will now have $Z = 2$ as the asymptotic charge. Second, the O_2^+ diatomic possesses parity symmetry, such that the number of angular momentum terms that contribute to the wave function expansion is half that for NO for the same $l_{\max}$.

In Figure 8, we present the partial cross section for the $k\sigma_g$, $k\pi_g$, and $k\delta_g$ continua. Each panel displays the partial cross sections for two different basis set constructions of the molecular potential of $O_2^{+\,+}$. Both hybrid Gaussian-DVR and pure DVR treatments are shown in each panel. A very similar behavior of the cross section energy dependence is seen in the $k\pi_g$ and $k\delta_g$ partial cross sections as was observed for NO. The $k\sigma_g$ ionization channel for molecular ion O_2^+, however, exhibits no resonance structure.

As with NO, a comparison of the hybrid method with the pure single-center expansion reveals better agreement in the $k\pi_g$ and $k\delta_g$ channels of O_2^+. For either molecular potential shown in Fig. 8, the resulting cross sections in the hybrid method or pure DVR overlap each other better than for NO for both of these channels. In the hybrid method, up to $l_{\max} = 6$ is included in the region beyond the nuclei, while up to $l_{\max} = 10$ is utilized in the pure DVR single center expansion. The most substantial difference between these two frameworks is again seen in the $k\sigma_g$ channel containing the nuclei. Although the behavior of this partial cross section is similarly structure-less and falls off with photoelectron energy, the magnitude of the cross section near threshold does vary significantly. While the hybrid Gaussian-DVR results for this example appear to be converged in both the inner and outer region descriptions, increasing the maximum angular momentum $l_{\max}$ for the pure DVR calculation reveals slow convergence at threshold towards the hybrid result. Without the resonance structure seen at low energy for NO, this convergence in increasing partial-wave contributions near the nuclei is observed to be monotonic and slow as the larger ionic character of the target and residual double cation would seem to indicate a stronger relative impact of the nuclear attraction.

The absolute MFPAD for photoionization of O_2^+ to produce a 10 eV photoelectron in the xz-plane for both parallel and perpendicular polarization directions is illustrated in Figure 8. In the $k\pi_g$ continuum populated by parallel linear polarization, near perfect agreement between the hybrid Gaussian-DVR and pure DVR results is found. The MFPAD reveals very similar behavior for this angular distribution as for NO, however now possessing parity symmetry. In the perpendicular polarization, we see once again the more prominent d-wave character lobes are given very closely by both treatments in magnitude and direction. The difference in the secondary lobes directed along the molecular axis is less prominent than was seen for NO, but still remains the largest distinction between the hybrid-DVR and pure single-center calculations.

IV. CONCLUSIONS

In this work, we have expanded our previous studies utilizing the hybrid representation with interior Gaussian functions and grid-based DVR functions for multi-center molecular targets to consider linear molecules with many more core electrons and heavier atoms. Comparison of the hybrid results with slowly convergent single center expansions involving only DVR functions to describe the molecular environment reveals the major advantage of employing a hybrid representation in efficiently describing the electronic coordinates for continuum problems. The key is the flexibility allowing for both proper treatment of the electronic cusp behavior at the nuclei addressed using Gaussian-type functions ubiquitous with quantum chemistry, and grid-based numerical approaches well-suited for describing the oscillatory electron dynamics far from the molecular center. Incorporation of Gaussian functions that serve to reconstruct the molecular static-exchange potentials has also been implemented in a pure grid-based approach to describe the continuum electron coordinates. Several mixed-basis two-electron integral classes previously enumerated are must be considered in either approach and have been specialized to frozen-core molecular orbital densities that can be output by many standard quantum chemistry packages.

The impact of the molecular environment description is observed to be sensitive to the location of the nuclei and the ability of the basis to accurately account for the consequences of multi-center targets. Directly examining the characteristics of the wave function description in each underlying representation reveals the ways in which the non-spherical nature of molecular geometry impacts the angular distributions observed in the molecular frame. This type of analysis can help complement and explain the observations from sophisticated experimental techniques that can probe the molecular environment through ionic-fragment kinematic reconstruction.

Evaluation of non-trivial molecular continuum states that fully captures the dynamics of photon impact with one electron is critical to bridge towards more correlated process. The good agreement between the single ionization cross section calculated for NO using this scheme with other theoretical results is encouraging for advancing towards being able to tackle molecular double ionization with such a framework.

Acknowledgments

This material is based upon work performed at the University of California Lawrence Berkeley National Laboratory and was supported by the U.S. Department of Energy, Office of Science, Division of Chemical Sciences of the Office of Basic Energy Sciences under Contract DE-AC02-05CH11231.

[1] L. Tao, C. W. McCurdy, and T. N. Rescigno, Phys. Rev. A **79**, 012719 (2009).
[2] V. V. Serov and B. B. Joulakian, Phys. Rev. A **80**, 062713 (2009).
[3] L. Tao, C. W. McCurdy, and T. N. Rescigno, Phys. Rev. A **82**, 023423 (2010).
[4] X. Guan, K. Bartschat, and B. I. Schneider, Phys. Rev. A **83**, 043403 (2011), ISSN 0301-0104.
[5] I. Sanchez and F. Martin, Journal of Physics B: Atomic, Molecular and Optical Physics **30**, 679 (1997).
[6] H. Bachau, E. Cormier, P. Decleva, J. E. Hansen, and F. Martn, Reports on Progress in Physics **64**, 1815 (2001).
[7] M. Venuti, P. Decleva, and A. Lisini, Journal of Physics B: Atomic, Molecular and Optical Physics **29**, 5315 (1996).
[8] H. van der Hart, M. Lysaght, and P. Burke, Phys. Rev. A **76**, 043405 (2007), URL `http://link.aps.org/doi/10.1103/PhysRevA.76.043405`.
[9] D. Toffoli, M. Stener, G. Fronzoni, and P. Decleva, Chemical Physics **276**, 25 (2002), ISSN 0301-0104.
[10] M. A. Morrison, N. F. Lane, and L. A. Collins, Phys. Rev. A **15**, 2186 (1977).
[11] T. N. Rescigno and A. E. Orel, Phys. Rev. A **25**, 2402 (1982).
[12] W. Vanroose, F. Martín, T. N. Rescigno, and C. W. McCurdy, Phys. Rev. A **70**, 050703 (2004).
[13] W. Vanroose, F. Martín, T. N. Rescigno, and C. W. McCurdy, Science **310**, 1787 (2005).
[14] W. Vanroose, D. A. Horner, F. Martín, T. N. Rescigno, and C. W. McCurdy, Phys. Rev. A **74**, 052702 (2006).
[15] J. Colgan, M. S. Pindzola, and F. Robicheaux, Phys. Rev. Lett. **98**, 153001 (2007).
[16] F. L. Yip, C. W. McCurdy, and T. N. Rescigno, Phys. Rev. A **81**, 053407 (2010).
[17] F. L. Yip, F. Martín, C. W. McCurdy, and T. N. Rescigno, Phys. Rev. A **84**, 053417 (2011).
[18] F. Yip, A. Palacios, T. Rescigno, C. McCurdy, and F. Martn, Chemical Physics **414**, 112 (2013).
[19] F. L. Yip, C. W. McCurdy, and T. N. Rescigno, Phys. Rev. A **81**, 063419 (2010).
[20] F. L. Yip, T. N. Rescigno, C. W. McCurdy, and F. Martín, Phys. Rev. Lett. **110**, 173001 (2013).
[21] T. N. Rescigno, D. A. Horner, F. L. Yip, and C. W. McCurdy, Phys. Rev. A **68**, 020701 (2005).
[22] F. L. Yip, C. W. McCurdy, and T. N. Rescigno, Phys. Rev. A **78**, 023405 (2008).
[23] C. W. McCurdy, M. Baertschy, and T. N. Rescigno, J. Phys. B **37**, R137 (2004).
[24] M. E. Smith, R. R. Lucchese, and V. McKoy, The Journal of Chemical Physics **79**, 1360 (1983).
[25] L. A. Collins and B. I. Schneider, Phys. Rev. A **29**, 1695 (1984), URL `http://link.aps.org/doi/10.1103/PhysRevA.29.1695`.
[26] M. Hermann, C. B. Jr., W. Huo, S. Langhoff, and P. Langhoff, Chemical Physics **109**, 1 (1986), ISSN 0301-0104.
[27] W. J. Hehre, R. F. Stewart, and J. A. Pople, The Journal of Chemical Physics **51**, 2657 (1969).
[28] A. Schafer, C. Huber, and R. Ahlrichs, The Journal of Chemical Physics **100**, 5829 (1994).
[29] V. I. Lebedev and D. N. Laikov, Dokl. Math. **59**, 477 (1999).
[30] T. N. Rescigno and C. W. McCurdy, Phys. Rev. A **62**, 032706 (2000).

Figures

FIG. 1: (Color online) Real part of the continuum wave functions constructed in the hybrid Gaussian-DVR basis for valence photoionization of NO resulting in a 10 eV photoelectron, plotted in the xz-plane (in atomic units, 1 a_0=5.29×10^{-9} cm). The molecular axis defines the z-axis with the N atom located at $z = -1.159$ bohr and the O atom at $z = +1.015$ bohr. Contour lines of the amplitude are plotted in the plane below. Upper panel shows the result for photon polarization parallel to the z-axis; lower panel displays x-axis polarization.

FIG. 2: (Color online) Partial photoionization cross sections of valence NO photoionization calculated with different static-exchange potentials of the closed-shell NO^+ ion (curves without symbols) with relatively minimal basis sets STO-3G and 6-31g, and using natural orbitals of neutral NO (curves with symbols) with more extended basis sets tzp and ccvdz. Other theoretical calculations shown: Schwinger variational [24] (circles), stars are Linear Algebraic approach [25] (stars).

FIG. 3: (Color online) Partial photoionization cross sections calculated using the hybrid Gaussian-DVR basis (solid curves) and a pure DVR single-center expansion (dashed curves). Ion orbitals of NO^+ (upper panel) and NO natural orbitals (lower panel) are shown, along with the SV calculation [24] for comparison.

FIG. 4: (Color online) Same as Fig. 1, with continuum solutions calculated with a pure-DVR single-center expansion basis. The parallel polarization results have up to $l_{\max} = 9$, while the perpendicular x-polarization results have up to $l_{\max} = 13$. (1 a_0=5.29×10^{-9} cm)

FIG. 5: (Color online) Contour plots of the continuum solutions shown in Figs. 1 and 4, constructed in the hybrid Gaussian-DVR basis (upper panels) and pure DVR single-center basis (lower panels), respectively. Panels on the left show photon polarizations parallel with the molecular axis, while the right panels correspond to perpendicular x-polarization. (1 a_0=5.29×10^{-9} cm)

FIG. 6: (Color online) Left panels: absolute molecular-frame differential cross section for photoionization of NO producing a 10 eV photoelectron. Right panels: normalized angular distributions (MFPADs) with the molecular orientation as shown. Parallel z-polarization (upper panels) and perpendicular x-polarization (lower panels) are shown for both hybrid Gaussian-DVR (solid curve) and for pure-DVR (dashed curve) results calculated using a ccvdz neutral NO core-orbital representation.

FIG. 7: (Color online) Same as Fig. 2, for photoionization of O_2^+ at its equilibrium internuclear distance. Upper and lower panels correspond to core-orbitals representations of O_2^{++} constructed from a double zeta (dz) and triple zeta plus polarization (tzp) basis.

FIG. 8: (Color online) Same as Fig. 6 for O_2^+ photoionization producing a 10 eV photoelectron. The core orbital representation is double-zeta orbitals of O_2^{++}.

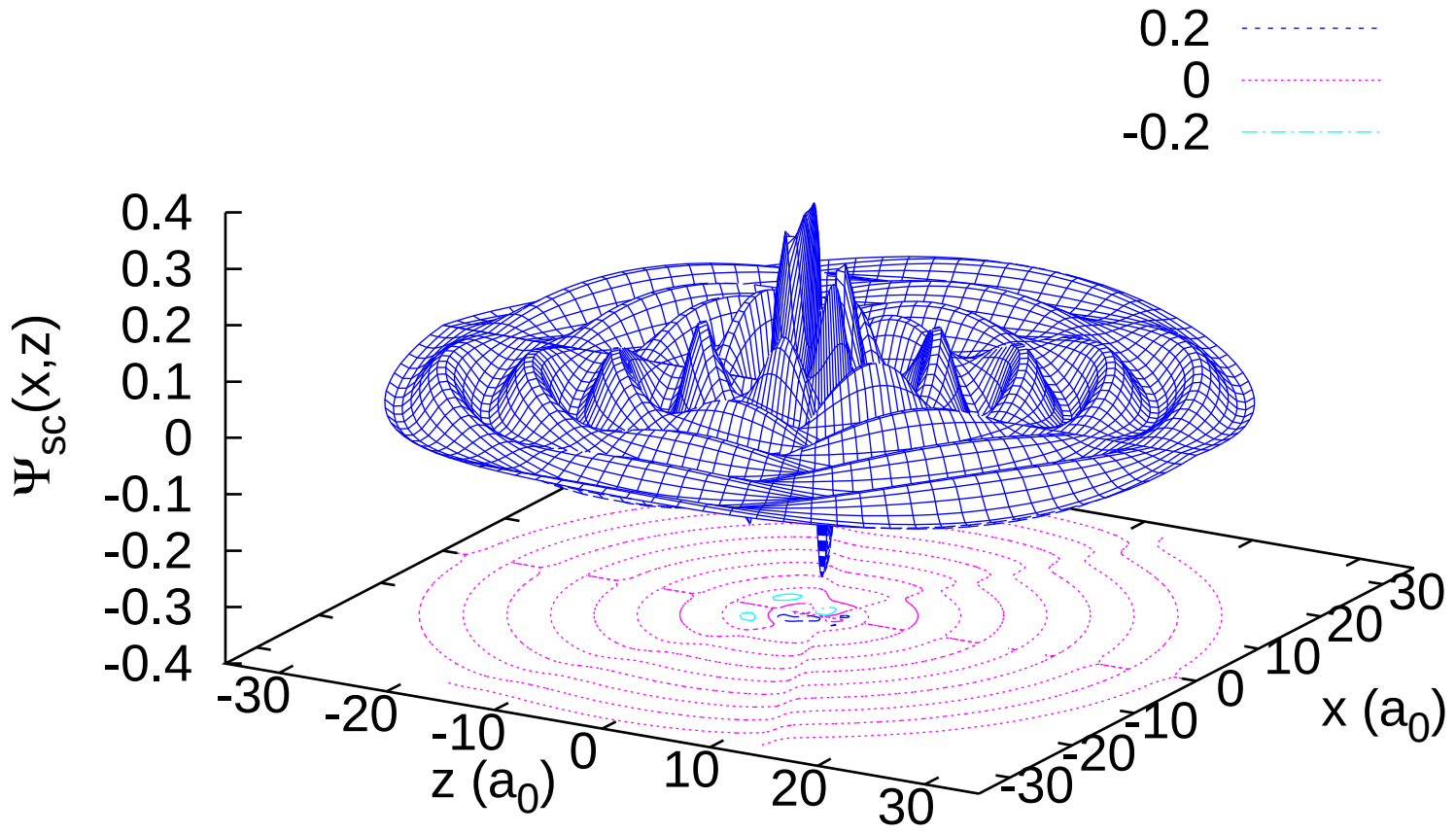

Figure 1a 03Dec2014

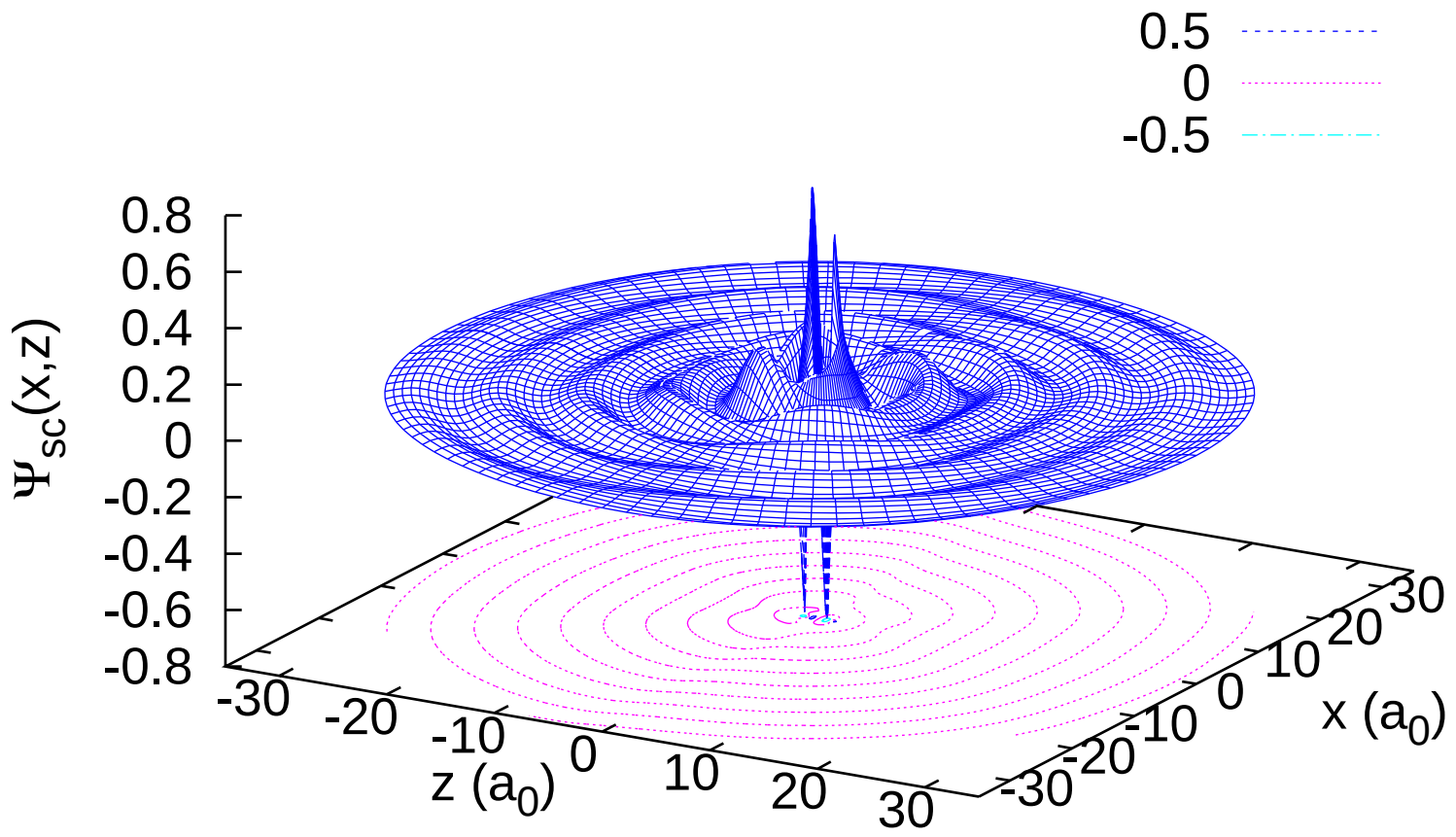

Figure 1b 03Dec2014

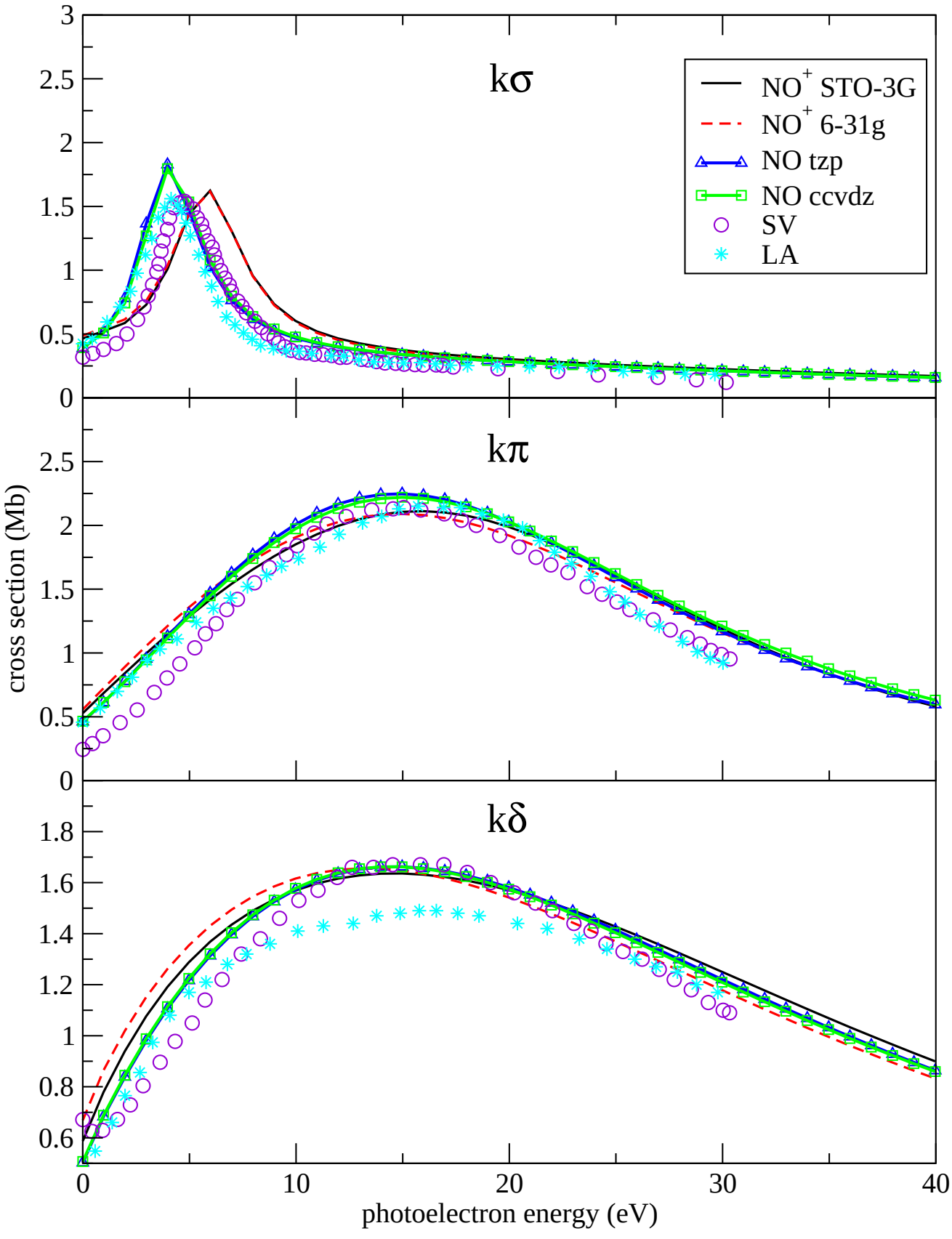

Figure 2 03Dec2014

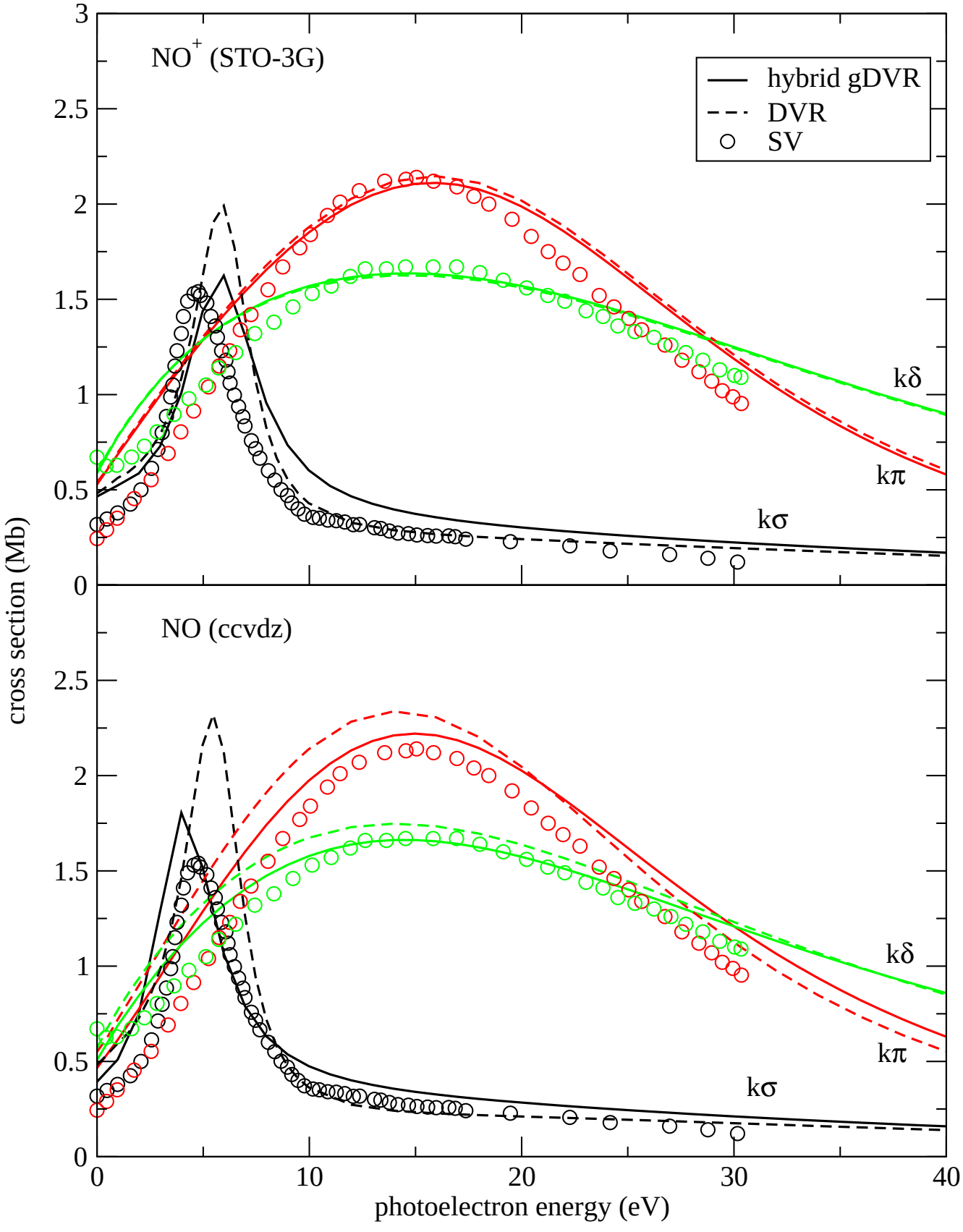

Figure 3 03Dec2014

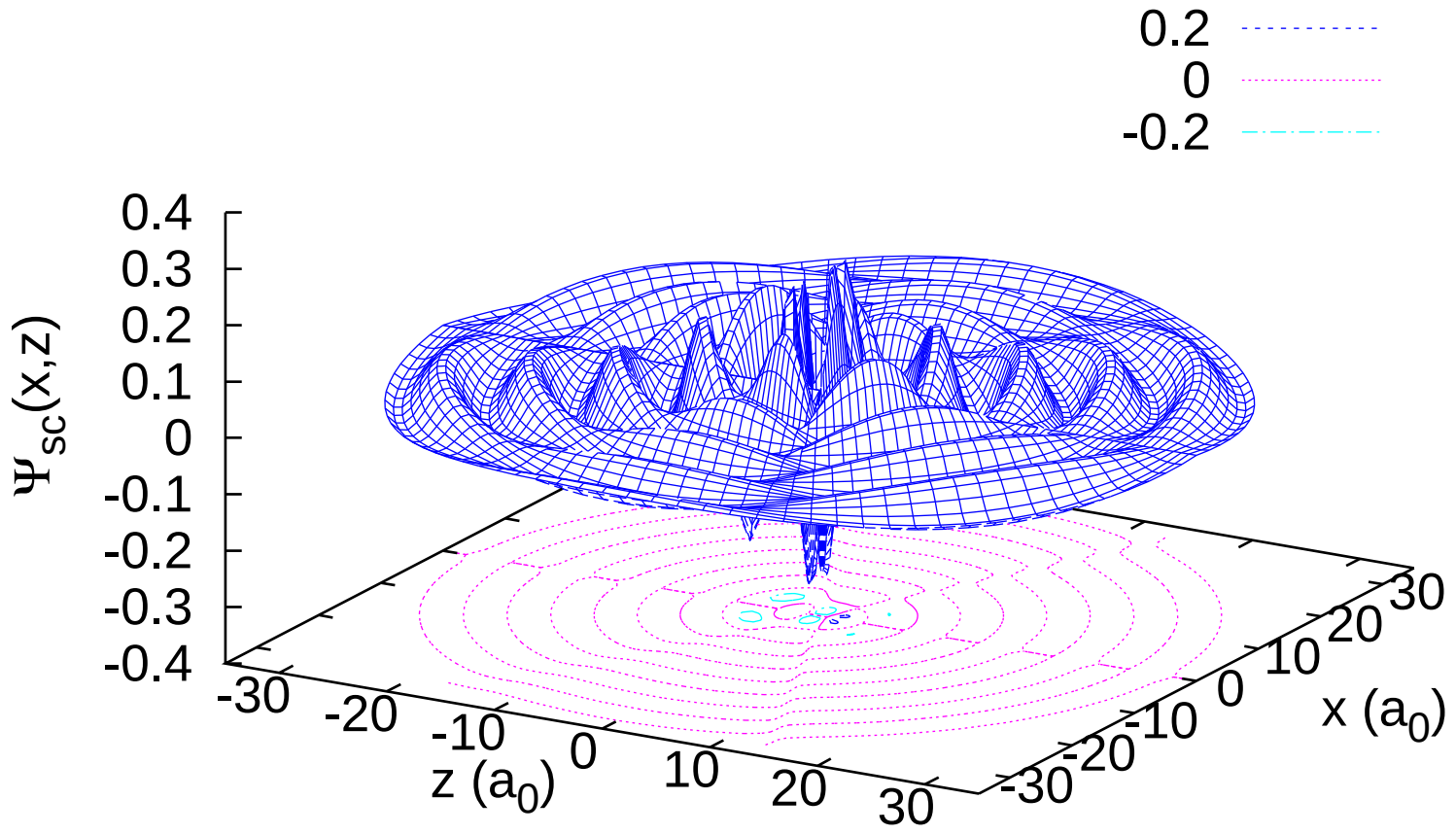

Figure 4a 03Dec2014

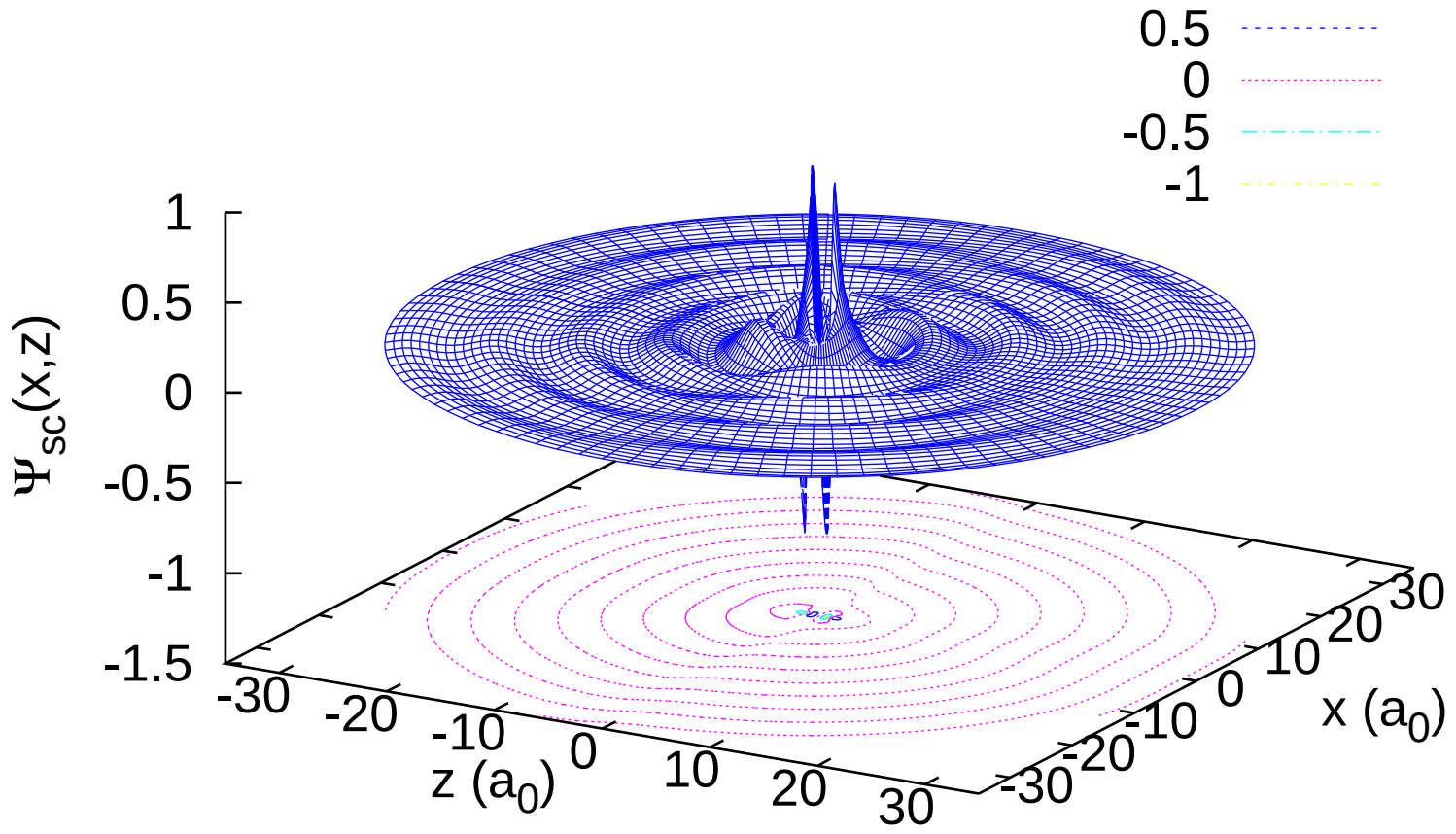

Figure 4b 03Dec2014

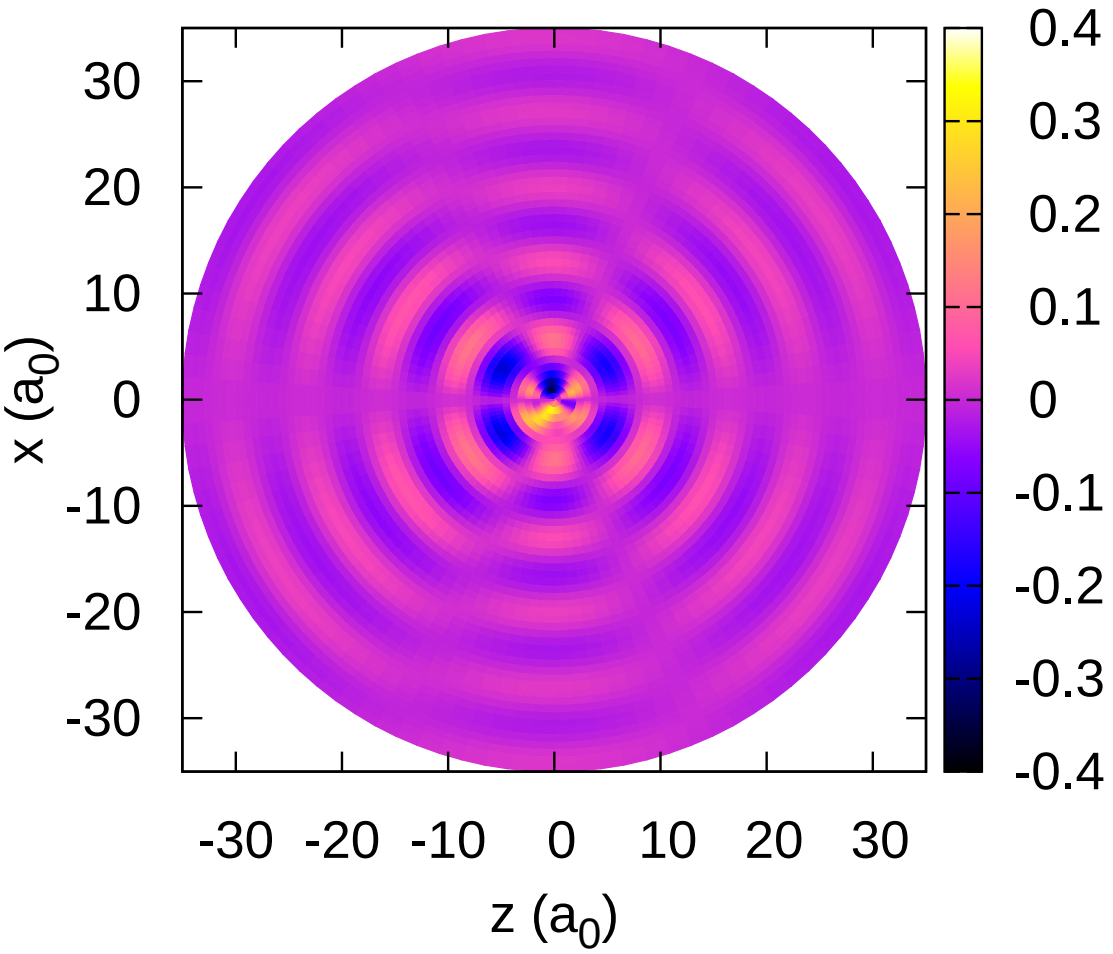

Figure 5a

03Dec2014

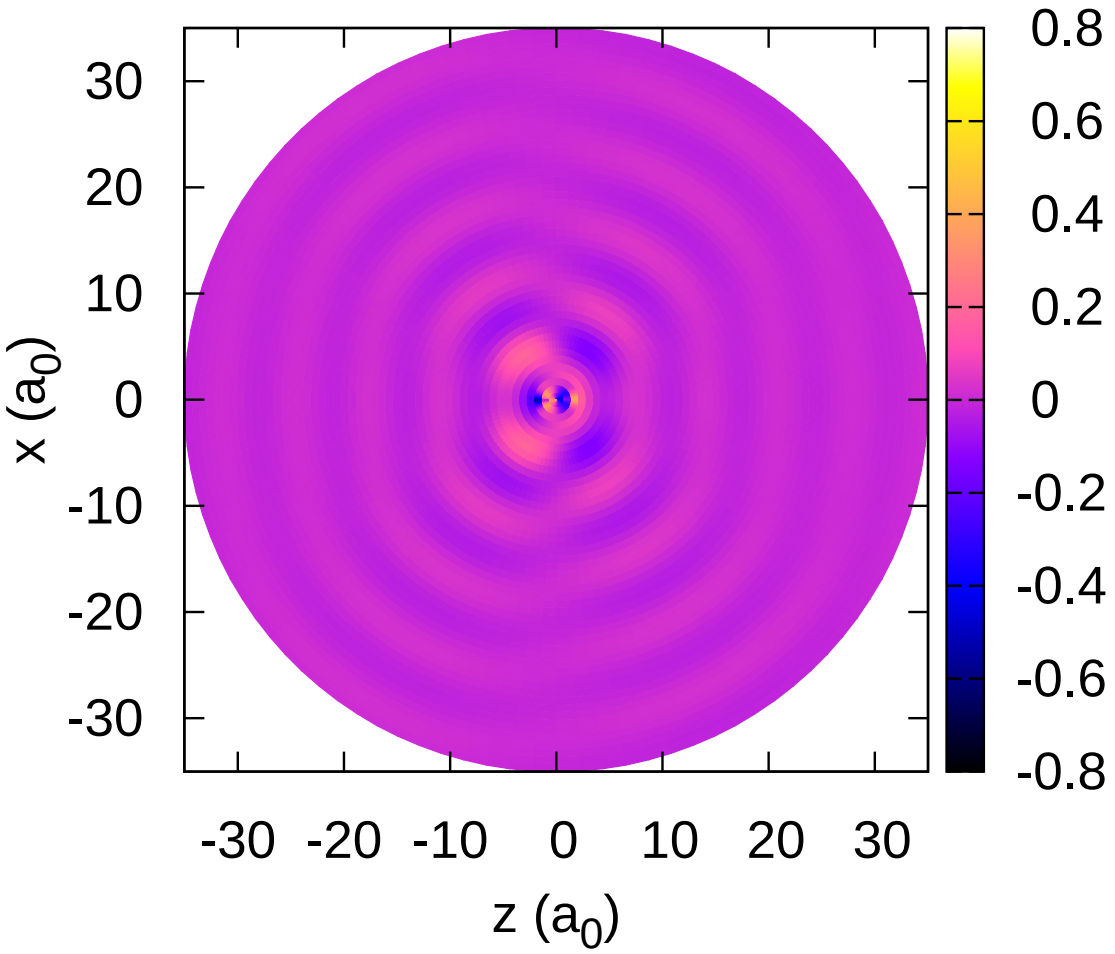

Figure 5b

03Dec2014

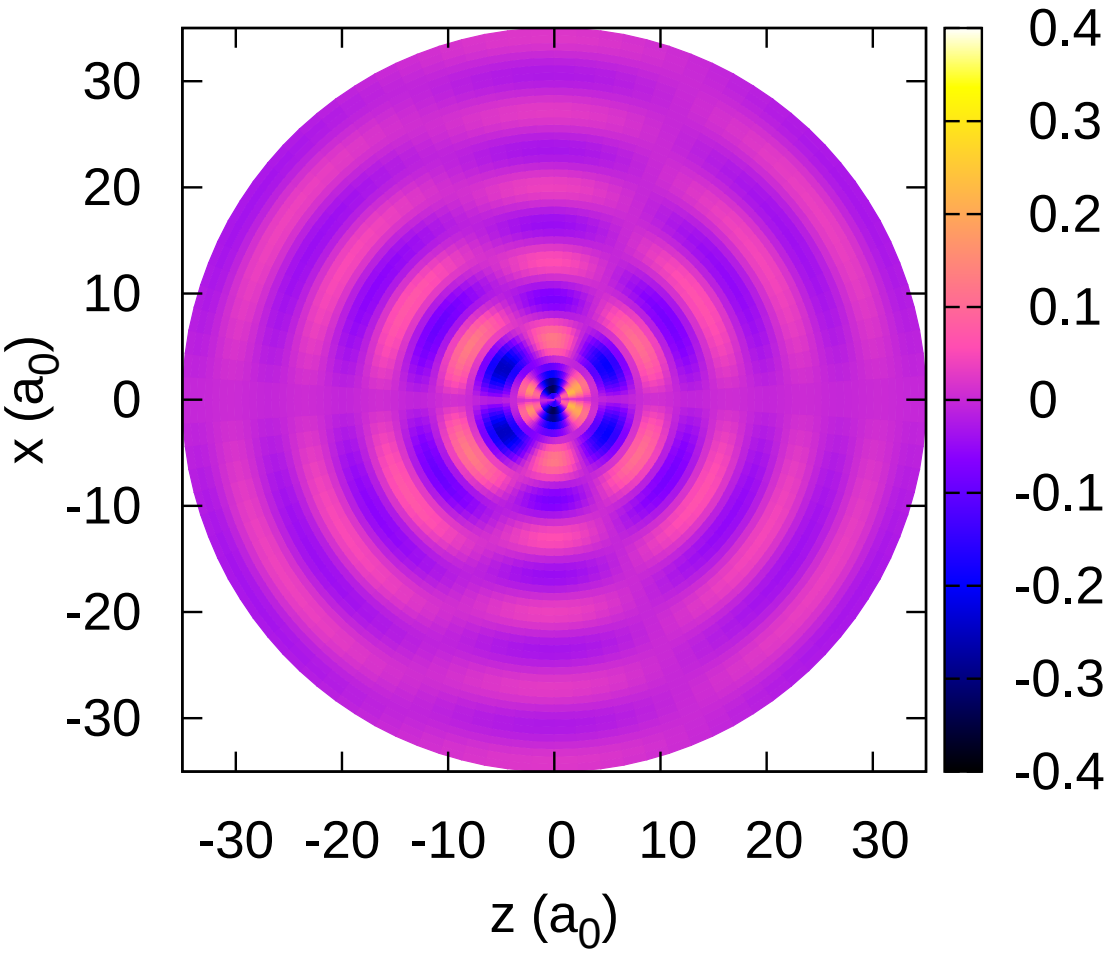

Figure 5c

03Dec2014

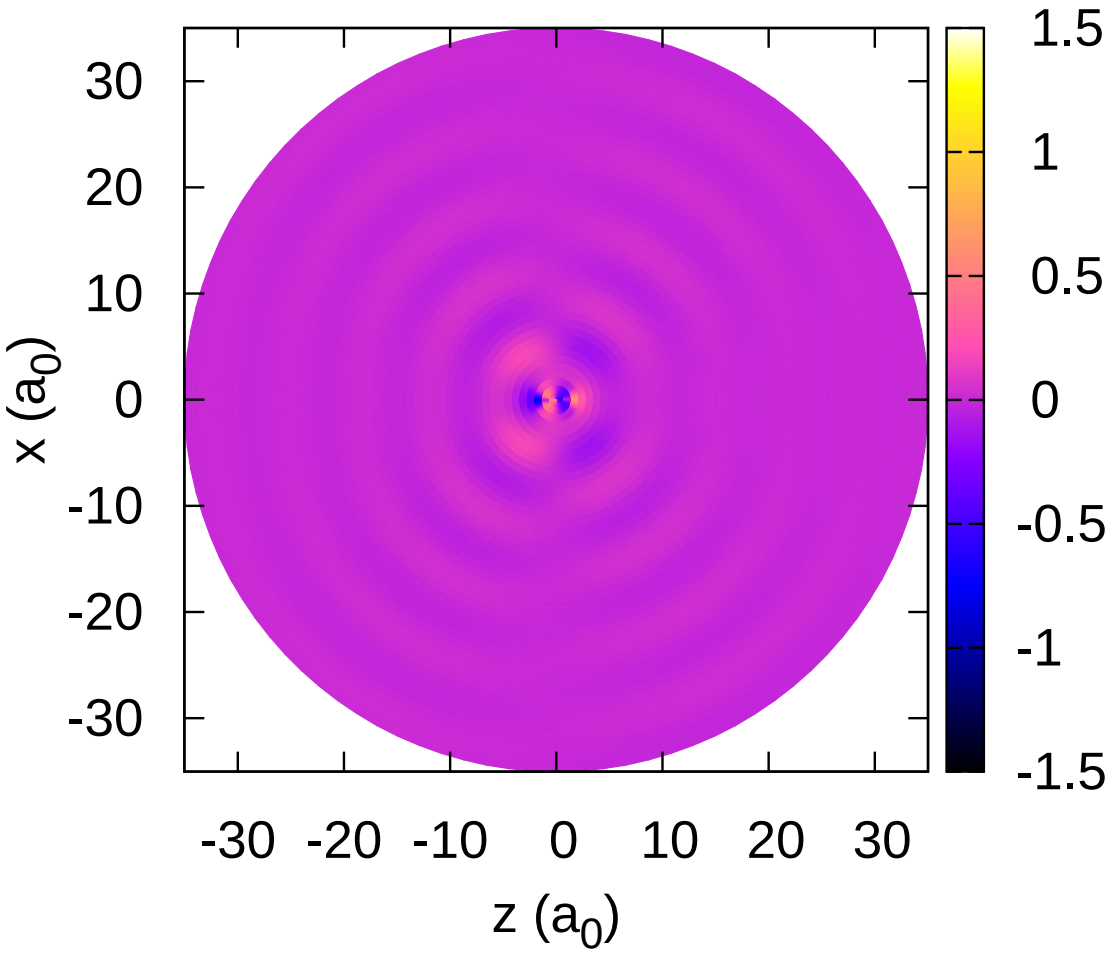

Figure 5d

03Dec2014

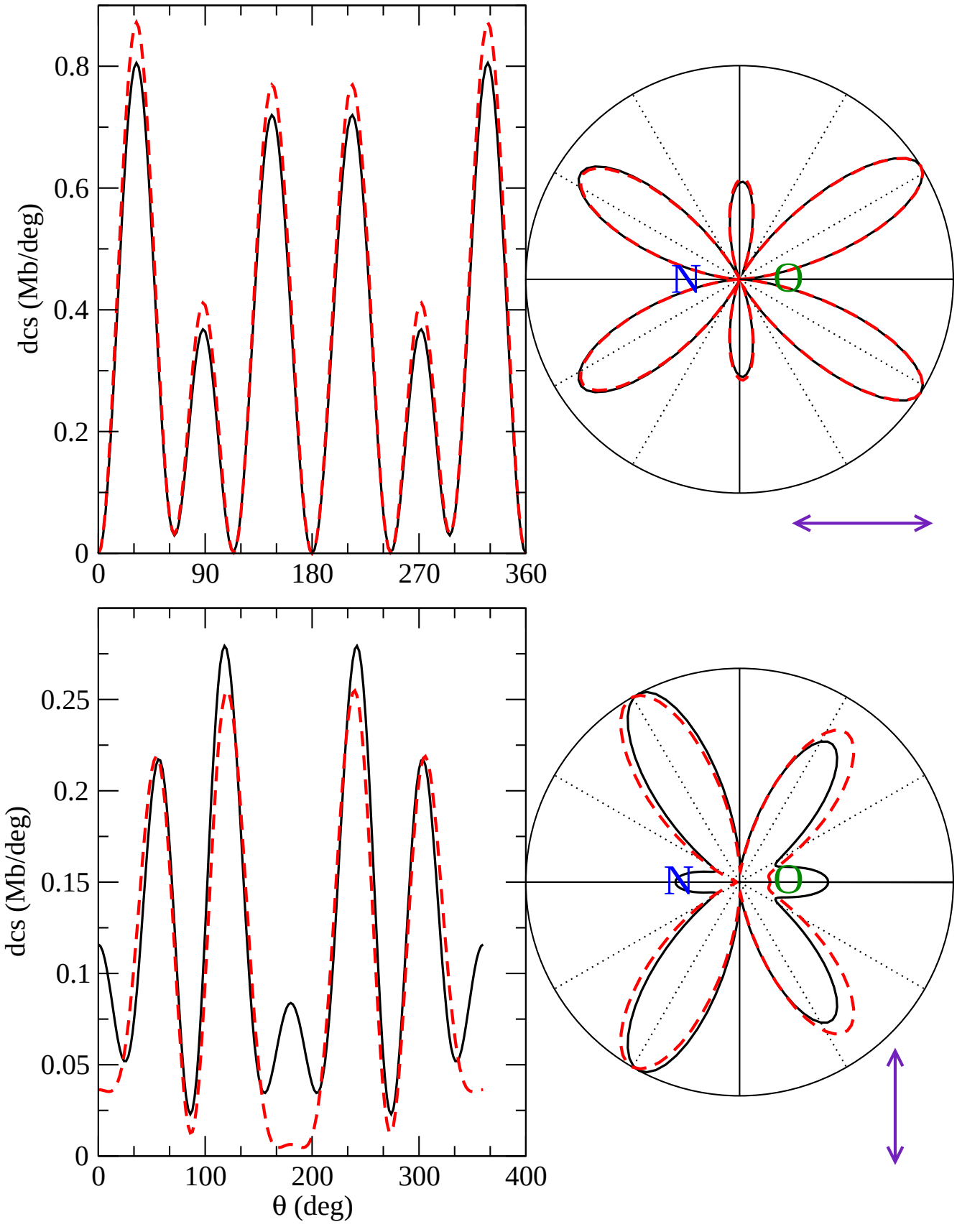

Figure 6 03Dec2014

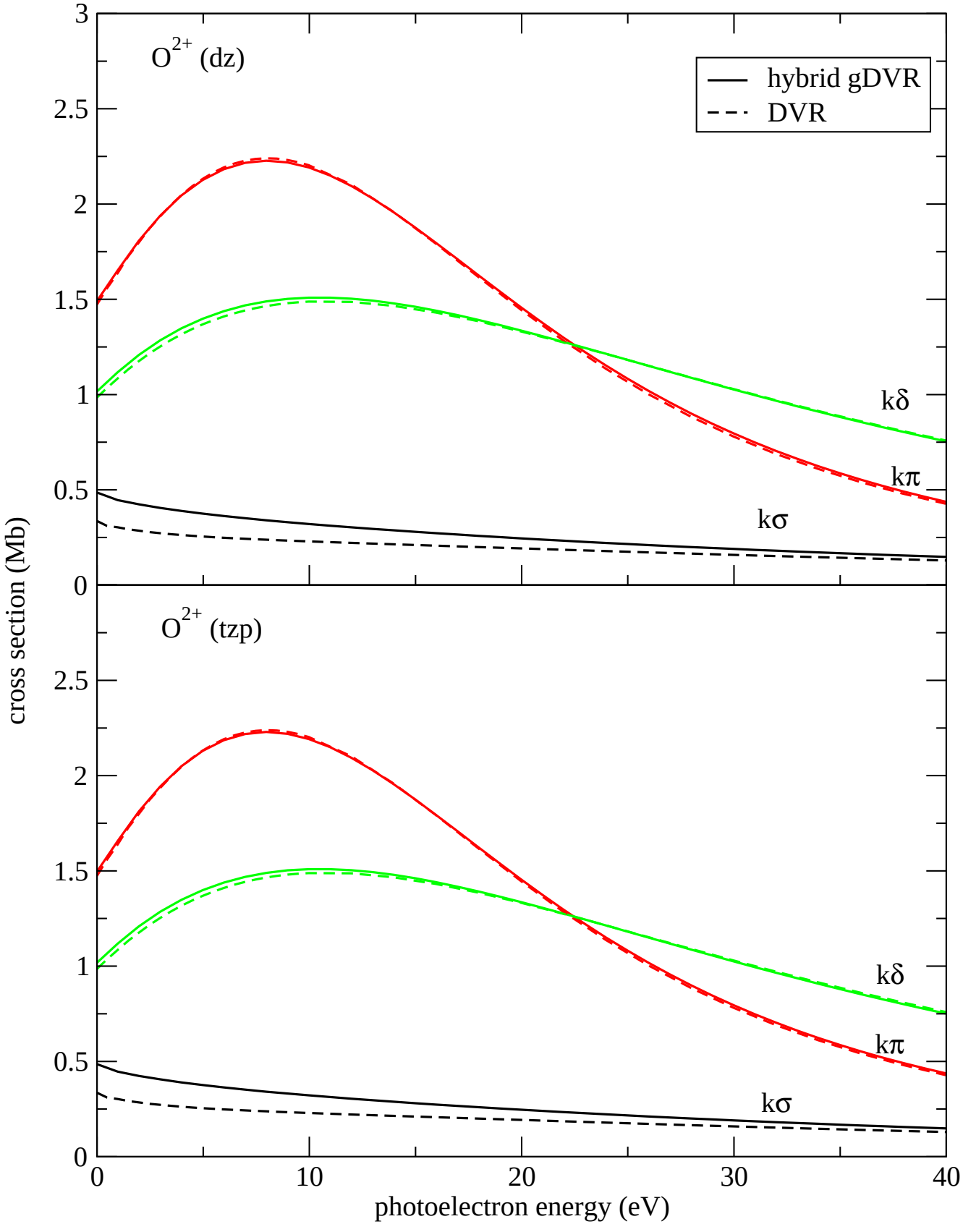

Figure 7 03Dec2014

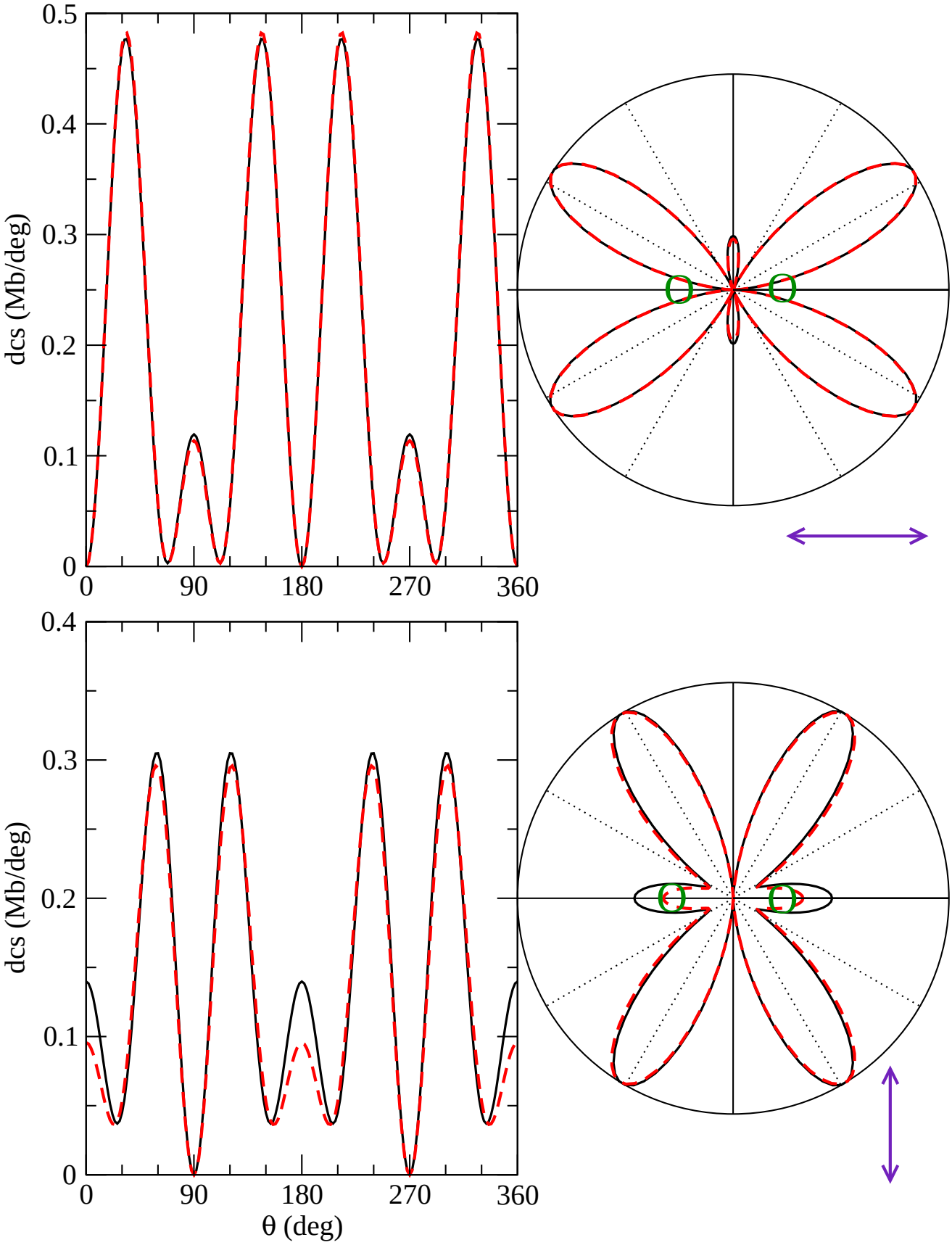

Figure 8 03Dec2014